Composites Part A 113 (2018) 311–317

Contents lists available at ScienceDirect

Composites Part A

journal homepage: www.elsevier.com/locate/compositesa

Realizing the theoretical stiffness of graphene in composites through confinement between carbon fibers

Jingwen Chu[a], Robert J. Young[a,*], Thomas J.A. Slater[b], Timothy L. Burnett[b], Broderick Coburn[c], Ludovic Chichignoud[d], Aurèle Vuilleumier[e], Zheling Li[a,*]

[a] National Graphene Institute and School of Materials, University of Manchester, Manchester M13 9PL, UK
[b] Henry Moseley X-ray Imaging Facility and School of Materials, University of Manchester, Manchester M13 9PL, UK
[c] McLaren Applied Technologies, McLaren Technology Centre, Chertsey Road, Woking, Surrey GU21 4YH, UK
[d] North Thin Ply Technology Sarl, Chemin du Closel 3, 1020 Renens, Switzerland
[e] RICHARD MILLE, Rue du Jura 11, CH-2345 Les Breuleux, Switzerland

ARTICLE INFO

Keywords:
A. Nanocomposites
A. Hybrid
B. Mechanical properties
Raman spectroscopy

ABSTRACT

It is shown that approximately 2 wt% of graphene in the matrix of a unidirectionally-reinforced carbon fiber epoxy composite leads to a significant enhancement in mechanical properties. Particularly, it is found that the axial stiffness of the composites is increased by ~10 GPa accompanied by an increase in axial strength of 200 MPa. X-ray computed tomography and polarized Raman spectroscopy have demonstrated that the graphene is predominately aligned parallel to the carbon fibers axes. Stress-induced Raman band shifts showed that the confined and self-aligned graphene is subjected to high levels of stress during axial deformation of the composite, with an effective Young's modulus of ~825 GPa, approaching its theoretical value of 1050 GPa. This behavior has been modeled using the rule of mixtures and shear-lag analysis and it is demonstrated that highly-aligned graphene in a constrained environment between fibers gives significantly better mechanical reinforcement than graphene in conventional polymer-based nanocomposites.

1. Introduction

Since graphene has high levels of stiffness and strength [1], its use as a reinforcement in polymer composites shows huge potential of further enhancing the mechanical properties of composites. Additionally, graphene can provide good electrical and thermal conductivity, improved thermal stability and sensing capabilities [2] in polymer composites even at low loadings [2–4]. The use of the commercially-available graphene nanoplatelets (GNP), usually few- or multi-layer graphene, retains reasonably good properties compared to exfoliated graphene, but it is much more cost effective.

Some of the early work in the graphene nanocomposites was carried out more than ten years ago by Stankovich et al. [5] by fabricating a graphene-reinforced polystyrene. They found that the electrical conductivity was increased by more than 10 orders of magnitude. Later the same group prepared a graphene oxide (GO) paper which achieved a Young's modulus as high as 42 GPa [6]. Since then, the study of graphene-based polymer nanocomposites has boomed but it was not until 2010 that the mechanical reinforcement mechanism was revealed by Gong et al. [7]. They showed that even as a one-atom thick material, graphene still follows continuum mechanics at the microscale. Later work from the same group demonstrated the dependence of reinforcement of graphene on its number of layers, which made the community aware of that monolayer graphene is probably not the optimal choice [8]. In addition, in terms of its spatial orientation, aligned graphene gives nearly double the reinforcement of the randomly oriented material [9,10], and this has also been found recently to affect the mechanical properties of hybrid composites by Leopold et al. [11]. However, although the theoretical Young's modulus of graphene was found to be around 1 TPa [1], it is extremely difficult to realize a modulus close to this value in polymer-based nanocomposites [12]. As reviewed recently [3], the effective modulus of graphene is found to scale with the stiffness of the polymer matrix [13], and is relatively low since the Young's modulus of most polymers is below 5 GPa.

Beyond the modification of polymers by using graphene alone, there are also demands at the high-end applications, such as in the aerospace and automotive sectors, which are still dominated by fibers for mechanical reinforcement. However, the modern structures in aerospace and automotive sectors are becoming lighter and thinner, but still require high levels of aerodynamic and vibration stability, leading to the

* Corresponding authors.
E-mail addresses: robert.young@manchester.ac.uk (R.J. Young), zheling.li@manchester.ac.uk (Z. Li).

https://doi.org/10.1016/j.compositesa.2018.07.032
Received 5 March 2018; Received in revised form 24 July 2018; Accepted 25 July 2018
Available online 26 July 2018

stiffness becoming a dominant design driver. Attempts have also been made to introduce graphene [14] and its derivatives GO [15–17] or functionalized GO [18] into fiber hybrid composites to improve various properties such as flexural behavior [17,18], ultimate tensile strength (UTS) [15], interfacial shear strength (IFSS) [14,15,18], interlaminar shear strength (ILSS) [15,18], fatigue property [19] and toughness [16]. However, only a few reports can be found regarding enhancing the Young's modulus of composites, and with only limited improvement reported [15,18,20] as it is thought to be dominated by the high modulus fibers with the contribution of the low modulus matrix being insignificant.

In this work, through the addition of only a small amount of graphene into the matrix, the mechanical properties of a unidirectionally-reinforced carbon fiber composite have been significantly enhanced. This study therefore presents a way of increasing the axial stiffness and strength of composites, and elucidating the mechanisms that lead to this reinforcement. Hence a simple method is introduced that is capable of giving rise to significant enhancement to the axial mechanical properties of fiber-reinforced composites using conventional processing methods.

2. Experimental

2.1. Materials and processing

The graphene used was the XT grade purchased from 2-DTech Graphene, Manchester, UK and used as received. The epoxy resin and hardener employed were NTPT ThinPreg^{TM} 513 system (NTPT). The cured epoxy resin has a density of 1.22 g/cm^3, and was found to have a Young's modulus of 4.1 GPa. The carbon fibers used in this work were PAN-based T700 fibers from Toray, Japan and quoted by the manufacturer as having a Young's modulus of 230 GPa and a diameter of 7 μm. For the graphene-modified epoxy, 2 wt% of graphene was added to the resin, followed by heating to 60 °C when the mixture was shear mixed at 200 rpm for 30 min, followed by sonication for 15 min. The nominal weight fraction of the carbon fiber is 62%, and the prepreging was done in NTPT but due to commercial confidentiality details are not disclosed here. The carbon fiber prepregs were cured by being first heated to 80 °C and stabilized there for about 30 mins. The autoclave pressure was then increased from 1 to 5 bars, followed by being heated to 120 °C. The samples were kept at 120 °C for 2 h followed by cooling down to room temperature.

2.2. Microstructure characterization

Optical microscopy was undertaken using a Nikon Eclipse LV100ND optical microscope. The volume fraction of carbon fibers in the composites was determined from the optical micrographs using the software ImageJ. The number of pixels per fiber cross section was determined and the number of fibers counted. The total pixels for all the carbon fibers was determined and divided by the number of pixels in the image to give the fiber volume fraction. The cross section of the composite specimens was prepared by grinding and polishing using grinding paper and polishing cloth. Scanning electron microscopy (Philips XL30 FEGSEM) was used to determine the position of the graphene in polished sections of the composites and the surfaces of the composites following fracture. In each case, the specimen surface was gold-coated before imaging. The X-ray diffraction (XRD) pattern was obtained using a PANalytical X'Pert Pro diffractometer with a Cu Kα radiation source. X-ray computed tomography (CT) was undertaken using a Zeiss Xradia 810 Ultra instrument, a lab based X-ray CT instrument using 5.4 kV energy X-rays that are focused using a Fresnel zone plate. The X-ray CT instrument was operated in large field of view phase contrast mode, in which a Zernike phase ring provides X-ray phase contrast. Reconstruction was performed in the Zeiss Xradia XMReconstructor software (version 9.1.12862), using their proprietary back projection based reconstruction algorithm. Visualization and analysis was performed in Thermo Fischer Avizo software (version 9.2.0), employing manual segmentation to analyze graphene platelets and carbon fibers. The orientation of the axial direction of the fibers and the normal direction of the graphene flakes were both determined in Avizo, using the Label Analysis toolbox. Subsequent analysis and plotting of the pole figures was performed in the Matlab toolbox MTEX (version 4.4). The dispersion and spatial orientation of the graphene in the composites were determined by Raman spectroscopy using a Renishaw inVia Raman spectrometer with a laser of wavelength $\lambda = 532$ nm and a laser spot size of around 1–2 μm in diameter. For the orientation test, the polarization of both the incident and scattered radiation were set parallel.

2.3. Mechanical testing

The mechanical testing was carried out using an Instron 5985 according to ISO527 Standard, with a 250 kN and 30 kN load cell for 0° and 90° unidirectional samples, respectively. Six samples for each of the 0° and 90° unidirectional composites were tested. Strain was measured using an extensometer, which was removed prior to specimen failure for the 0° samples to avoid damage. Shifts of the Raman bands for the graphene in the composites under stress were followed using a Horiba LabRAM HR Evolution ($\lambda = 488$ nm). For the bending test, both unpolished and polished graphene–enhanced composite specimens were placed in a four-point bending rig, and deformed by step-by-step bending. The strain was determined using a strain gauge attached to the sample surface [21]. The polarization of the laser was kept parallel to the tensile strain direction, in both the 0° and 90° tests.

3. Results and discussion

Full characterization of the different component materials used in the composites was undertaken as shown in Fig. 1. Fig. 1a shows a scanning electron microscope (SEM) image of the XT graphene powder that was found to have lateral dimensions of ~5–10 μm. The XRD pattern shows $2\theta = 26.4°$, corresponding to an interlayer spacing ~0.34 nm (Fig. 1b). This is further confirmed by the position of the symmetric 2D band at ~2700 cm^{-1} in the Raman spectrum from the XT graphene powder (Fig. 1c) showing that it is few-layer graphene (~5 layers) [22,23]. This is a typical example of exfoliated graphene with a relatively low defect density, as indicated by the low intensity of the Raman D band [24]. The Raman spectra of the neat epoxy and T700 carbon fiber are also shown in Fig. 1c. The spectrum of the carbon fiber has broad D and G bands, in accordance with the turbostratic structure of PAN-based carbon fibers [25]. The Raman spectrum of the epoxy resin shows a number of peaks on a fluorescence background.

The dispersion of the graphene in the enhanced epoxy composite was examined as shown in Fig. 2 and SI. It was quantified by using the intensity of the graphene Raman 2D band (I_{2D}) (Fig. 2a). Fig. 2b & c show that the graphene is well dispersed within the fiber-reinforced composite, where a lighter color corresponds to a higher value of I_{2D} thus higher concentration of graphene. It can be seen that graphene tends to be present between the gaps of the carbon fibers – a filtering effect. Higher magnification (Fig. 2d & e) shows a graphene flake being sandwiched between two fibers. The dispersion of the graphene was also analyzed by using X-ray CT scans. Both the spatial arrangement of the graphene and its relationship to the fibers are clearly shown (Fig. 2f). The majority of the graphene flakes are aligned parallel to the fibers with a misorientation within ± 20°, as shown as the blue dots in the pole figure (inset in Fig. 2f). The close proximity and alignment of the flakes to the fibers suggest that the graphene flakes were aligned when the graphene/epoxy mixture passed through the narrow gaps between the fibers. It appears that this orientation was maintained during curing, leading to flat graphene flakes appearing to be attached to the fibers [26], as confirmed by the SEM image of the fracture surface

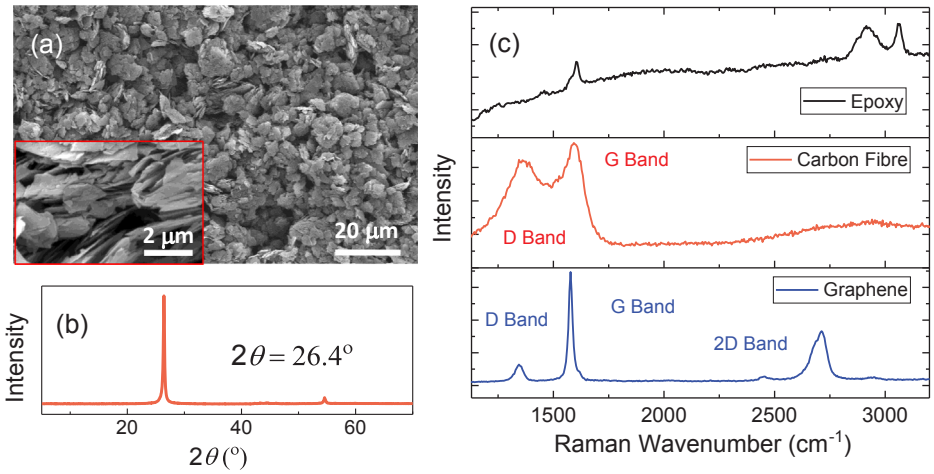

Fig. 1. (a) SEM micrograph of the graphene flakes. Inset is the image at high magnification. (b) XRD pattern of the graphene powder. (c) Raman spectra of the epoxy resin, T700 carbon fiber and graphene flakes. (For interpretation of the references to colour in this figure legend, the reader is referred to the web version of this article.)

of the composite shown in the SI (Fig. S2c).

Supplementary data associated with this article can be found, in the online version, at https://doi.org/10.1016/j.compositesa.2018.07.032.

In addition to the X-ray CT scan, the spatial orientation of graphene has also been quantified by using polarized Raman spectroscopy, based on the previous report [9,10] that I_{2D} is a maximum/minimum when the laser polarization is parallel/perpendicular to the graphene plane. The sample was set up as shown in Fig. 3a and the polarized laser was parallel to either the Y or Z axes. With the sample rotated, the variation of I_{2D} as the function of $\Phi_{Y/Z}$ can be obtained. Details of the model can be found in the SI and Ref. [9]. Briefly, the spatial orientation of graphene can be quantified by fitting the variation of I_{2D} as the function of $\Phi_{Y/Z}$ by two parameters $\langle P_2(\cos\theta)\rangle$ and $\langle P_4(\cos\theta)\rangle$ using Eq. S1 and it can be further correlated with the Young's modulus of the composites by using the Krenchel orientation factor η_o [27]. The value of η_o has been calculated to be '1' for perfect spatial orientation and '8/15' for random alignment for two-dimensional flakes [10]. Routinely the variation of I_{2D} in the Y and Z directions is used to predict η_o in the Y/Z direction (Y and Z are equivalent) by using Eq. (1), but adjusting the analysis also enables η_o in the X direction to be revealed:

$$\eta_o(Y/Z) = \frac{8}{15} + \frac{8}{21}\langle P_2(\cos\theta)\rangle + \frac{3}{35}\langle P_4(\cos\theta)\rangle \quad (1)$$

$$\eta_o(X) = \frac{8}{15} - \frac{16}{21}\langle P_2(\cos\theta)\rangle + \frac{8}{35}\langle P_4(\cos\theta)\rangle \quad (2)$$

The results obtained are shown in Fig. 3b and c. As the Y and Z directions are equivalent, they both show similar η_o values for the Y/Z directions of ~0.40, and X direction of ~0.80. This demonstrates that the graphene flakes are aligned almost uniformly around the X axis with their surface normals roughly perpendicular to the X axis [28], as drawn schematically in Fig. 3d, supporting the 'filtering' effect hypothesis as discussed before. This orientation was maintained during curing hence leading to the graphene being sandwiched between fibers

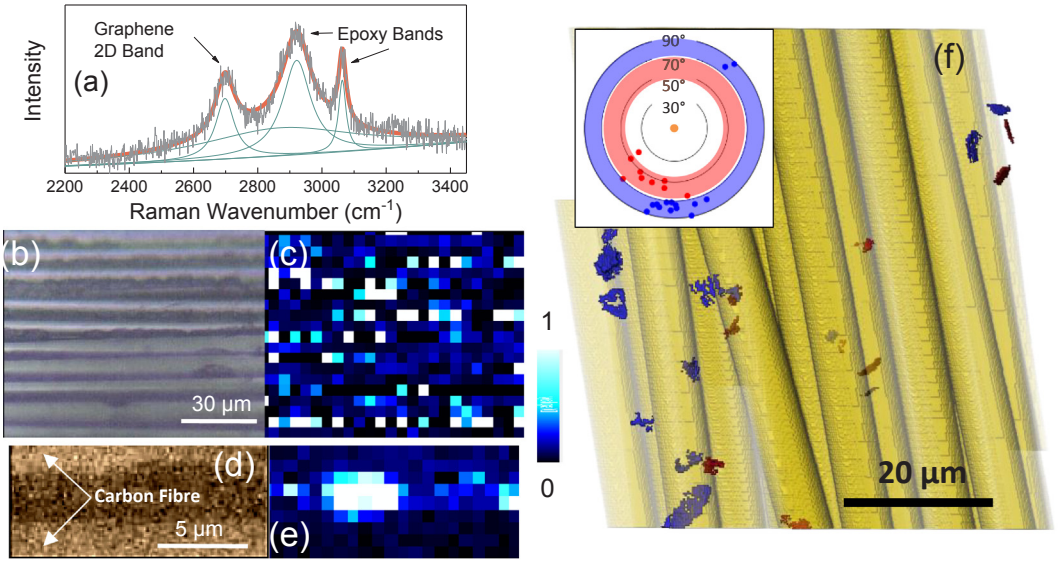

Fig. 2. (a) Raman spectrum showing the method of determining the Raman band intensities for the graphene and epoxy resin. The grey, red and green lines are the original spectrum, curve fitting for the spectrum and individual bands, respectively. (b) Optical micrograph and (c) Raman map of the variation of I_{2D} in the same area. (d) Optical micrograph and (e) Raman map of the variation of I_{2D} in the same area of a graphene flake being sandwiched between two carbon fibers. (c) and (e) share the same color bar showing the normalized I_{2D}. (f) Segmented 3D volume rendering of the reconstructed X-ray CT data showing the spatial arrangement of the carbon fibers and graphene. The graphene flakes are artificially colored such that the blue ones represent flakes within ± 20° parallel to the fibers (determined from the surface normal), while the red ones are outside this range. The inset is the pole figure generated accordingly, where the orange dot represents the average axial direction of fibers, and the blue and red dots denote the surface normal of the blue and red flakes in (f). The numbers indicate the angle between the surface normal of graphene and fibers. The blue and red shadows are the guide to eyes on the average orientation direction of the blue and red dots, respectively. (For interpretation of the references to colour in this figure legend, the reader is referred to the web version of this article.)

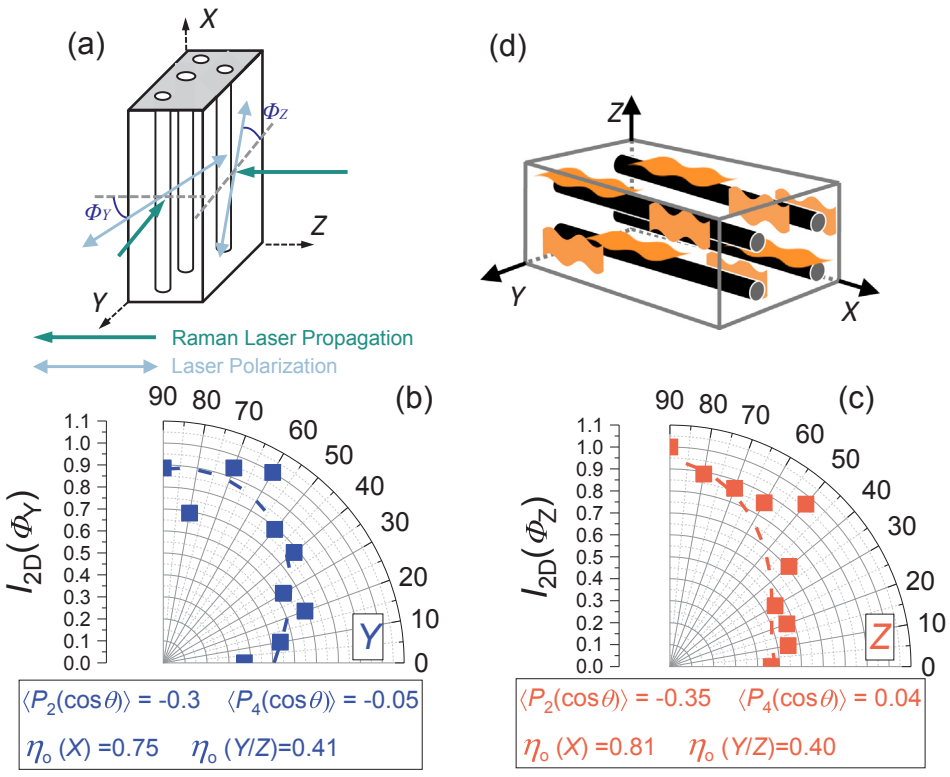

Fig. 3. (a) Experimental set up of the Raman orientation test. A representative measurement showing the I_{2D} variation as the function of (b) Φ_Y and (c) Φ_Z with the corresponding $\langle P_2(\cos\theta)\rangle$, $\langle P_4(\cos\theta)\rangle$ and η_o values shown. The dashed lines are the curve fittings using Eq. S1. (d) 3D illustration of the spatial orientation and conformation of the graphene. (For interpretation of the references to colour in this figure legend, the reader is referred to the web version of this article.)

as shown in the polished transverse section shown in Fig. 4, and also the fibers coated with flat graphene [26] on the fracture surface of the composite (Fig. S2c).

The mechanical properties of both the unenhanced and graphene-enhanced composites were determined by tensile testing and the stress-strain curves are shown in Fig. 5. The Young's modulus and ultimate tensile strength (UTS) were determined by deforming two types of specimens, one with the carbon fibers in the axial direction (0°) and the other with the fibers in the transverse direction (90°), using 6 specimens in each case. The results and their standard deviations are summarized in Table 1.

The volume fraction of the carbon fibers in the composites was carefully determined using optical microscopy from polished transverse sections as shown in the SI. It was found that the volume fractions of the carbon fibers measured in both the unenhanced and enhanced composites are very similar (~52%, Table 1), in good agreement with the nominal fiber content. Hence any differences in mechanical properties in the enhanced composites must be due to the presence of the graphene. For the composites with the carbon fibers in the axial direction (0°), Table 1 shows that the addition of the graphene leads to a significant increase in the Young's modulus of the order of 10 GPa and an increase in the UTS of around 200 MPa. In contrast, for the specimens with the fibers in the transverse direction (90°), there is only a very slight increase in both the Young's modulus and UTS, both of which are unchanged within the experimental error.

The mechanisms leading to the increase in the Young's modulus of the enhanced composite were investigated using Raman spectroscopy [7,29]. It is known that the Raman D [21,30], G [31] and 2D [7,16,31] band positions of graphene shift when the graphene is strained and the rate of shift per unit strain can be used to measure the stress in the graphene from knowledge of the Grüneisen parameter [16,31]. For the graphene studied in this work, it was found that the shift of the G band was the most convenient to follow because it is sharp and allows more accurate measurement than the other bands. It is worth noting that apart from the strain effect, doping from the environment may also induce the G band to shift. However, doping only induces G band to upshift [32], which contrasts with the G band downshift in this work resulted from strain. Also because the applied strain may lead to a

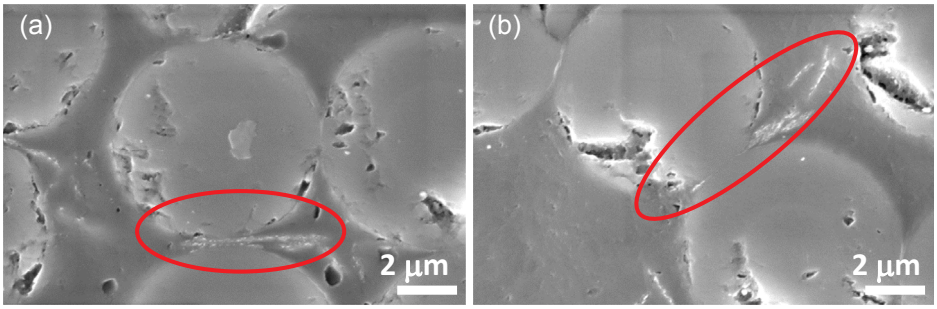

Fig. 4. SEM micrographs of polished sections of the graphene-enhanced composite showing graphene flakes (highlighted) confined between the carbon fibers. (For interpretation of the references to colour in this figure legend, the reader is referred to the web version of this article.)

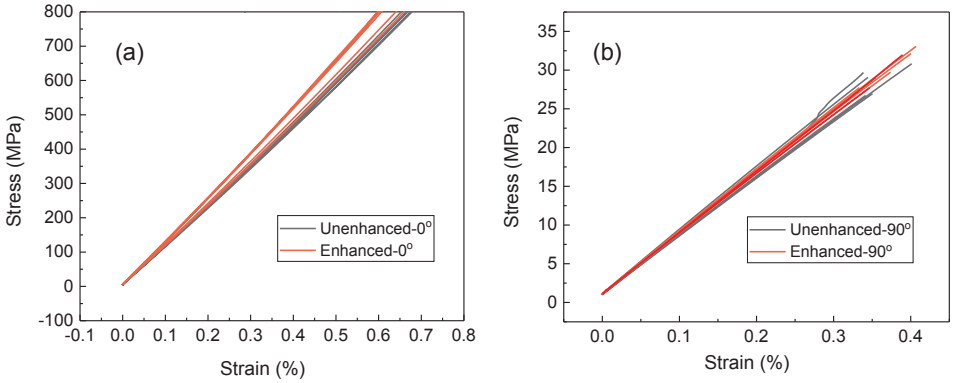

Fig. 5. Tensile stress-strain curves of the composites deformed in the (a) 0° and (b) 90° directions relative to the fiber axes. (For interpretation of the references to colour in this figure legend, the reader is referred to the web version of this article.)

Table 1
Mechanical testing results for both the unenhanced and enhanced composites. (The ± error bars are standard deviations.)

	Unenhanced	Enhanced
Fiber content (vol%)	52.5 ± 2.4	51.8 ± 0.6
0° Young's modulus (GPa)	114.5 ± 1.4	124.1 ± 5.1
0° UTS (MPa)	2418 ± 151	2636 ± 114
90° Young's modulus (GPa)	7.8 ± 0.3	7.9 ± 0.1
90° UTS (MPa)	29.1 ± 1.9	30.4 ± 2.3

stronger interaction between graphene and the matrix thus higher level of doping [33], where G band upshifts, it can be expected when the graphene is under tensile strain, the G band should initially downshift linearly but then flattens as strain increases. This is in contrast with this work where a linear G band downshift with the strain can be observed.

The deformation of the graphene in the enhanced composites was examined as outlined in Fig. 6 for the 0° sample. The specimens were deformed in a four-point bending rig where the strain ε was applied in the X direction with the incident laser along the Z axis (Fig. 6a). The change in the graphene G band position from the value at 0% strain ($\Delta\omega_G$) is shown as a function of ε in Fig. 6b. As the fiber-reinforced composite was polished to expose the graphene, some of the graphene was loosened or damaged by the polishing process. Hence only the 10 sets of measurements where the ω_G shift data had a value of the coefficient of determination $R^2 > 0.6$ are displayed. It can be seen that averaging the measurements from 10 sets of data gives an average value of $d\omega_G/d\varepsilon$ of $-21.2\,cm^{-1}/\%$, which is only slightly less than that of monolayer graphene, $\sim -27.0\,cm^{-1}/\%$ [31]. As the value of ω_G shifts with strain, this indicates that the graphene in the hybrid composites becomes highly strained. Hence good reinforcement from the graphene can be expected. It was also possible to measure the distribution of strain along a well-aligned graphene flake as shown in Fig. 6c. It can be seen that although there is scatter in the data the strain increases to

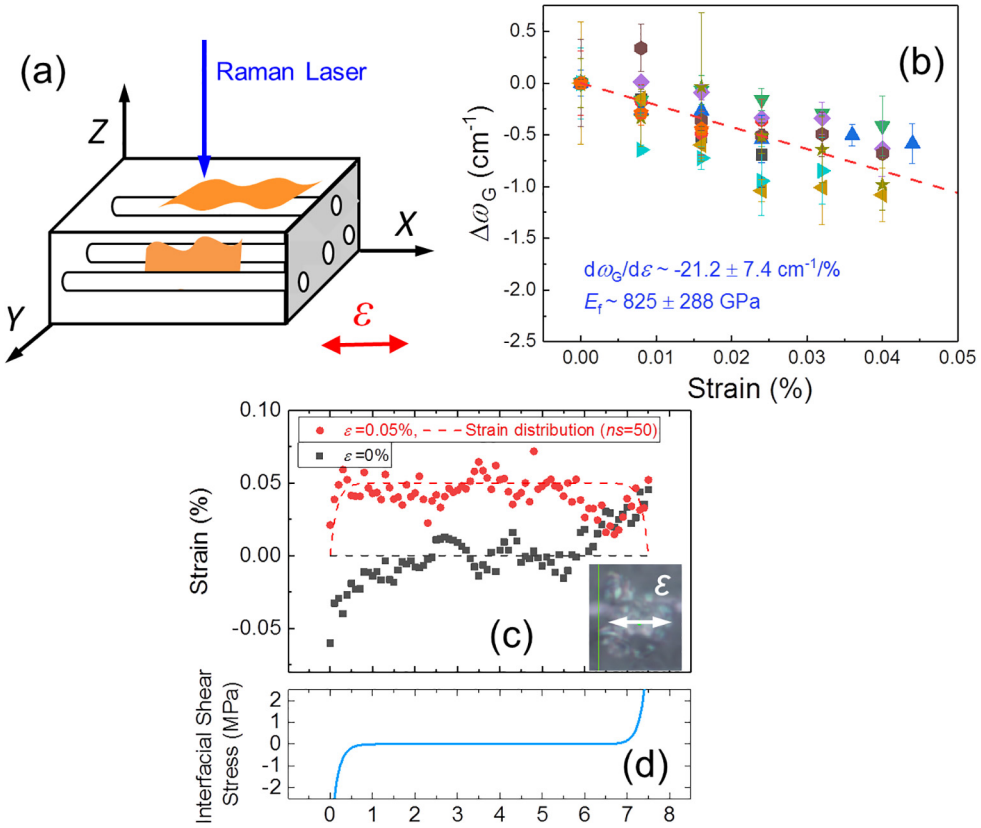

Fig. 6. Deformation of the graphene in the enhanced composites. (a) Deformation geometry showing the direction of applied strain, ε. (b) Change in Raman G-band position with strain. The points with same color belong to one set of measurement, and the slope is the average of the slopes of the 10 sets of experiments (red dashed line). (c) Distribution of strain along an embedded flake (inset) before and after deformation to 0.05% strain. (d) The distribution of interfacial shear stress along the flake modeled using shear-lag theory [7]. (For interpretation of the references to colour in this figure legend, the reader is referred to the web version of this article.)

approximately 0.05% along the flake on the application of a strain of 0.05%. The distribution of strain along the flake has been modeled using shear-lag theory in a similar manner to that undertaken by Gong et al. [7] for an isolated graphene monolayer, according to which a maximum interfacial shear stress of the order of 2 MPa is derived at the end of the flake (Fig. 6d).

The effective Young's modulus of graphene in the enhanced composite (E_f) can be estimated from the value of $d\omega_G/d\varepsilon$ determined in Fig. 6b. By comparing the measured value with the reference value ($(d\omega_G/d\varepsilon)_{Ref} \approx -27\,cm^{-1}/\%$) [31] obtained using the knowledge of Grüneisen parameter [8,21] it is given as

$$E_f = \frac{d\omega_G/d\varepsilon}{(d\omega_G/d\varepsilon)_{Ref}} \times E_{gra} \quad (3)$$

where E_{gra} is the Young's modulus of monolayer graphene ≈1050 GPa [1]. As per Eq. (3), the average value obtained of $d\omega_G/d\varepsilon = -21.2 \pm 7.4\,cm^{-1}/\%$ corresponds to an E_f of 825 ± 288 GPa (Fig. 6b). This shows that the reinforcement efficiency of the graphene in the hybrid composites approaches the theoretical value for monolayer graphene, indicating that the flakes remain intact during deformation and there is a strong interface between the graphene flakes and the composite matrix [3]. It should be pointed out, however, that the value of E_f is still slightly lower than E_{gra}, possibly due to the finite length [16] and inefficient interlayer stress transfer of the graphene [8].

The very high Raman band shift rate and value of E_f for the graphene in the enhanced fiber reinforced composite should be contrasted with the behavior of 'neat' graphene/epoxy nanocomposites, reinforced only with graphene, where shift rates of the order of $d\omega_{2D}/d\varepsilon \sim -5\,cm^{-1}/\%$ have been measured for the 2D band, giving a value of E_f in the order of only 70 GPa [13]. In the 'neat' graphene/epoxy nanocomposites, graphene is usually randomly oriented, crumpled and wrinkled in the matrix which compromises E_f [26,34]. The Raman band shift rate was also measured on the graphene at the surface of unpolished composites sample, which was close to the mould and hence resin rich (see Fig. S4 in SI). In this environment the graphene is less constrained and so the band shift rate is lower.

As the carbon fibers and epoxy resin matrix are subjected to uniform strain in 0° UD composites [35], a simple rule of mixtures can be employed to estimate the elastic properties of the composites. The Young's modulus of the unenhanced carbon-fiber/epoxy composite is then given by

$$E_{comp} = E_{CF}V_{CF} + E_{epoxy}V_{epoxy} \quad (4)$$

where E_{comp}, E_{CF} and E_{epoxy} are the Young's modulus of composite, carbon fiber and epoxy, respectively. V_{CF} and V_{epoxy} are the volume fraction of carbon fiber and epoxy, respectively. Although the nominal value of E_{CF} for T700 is 230 GPa, a calculation based on Eq. (4) using the value of E_{comp} for the unenhanced samples in Table 1 yields a value of $E_{CF} \approx 215$ GPa, with this slight reduction in comparison to the nominal value possibly being due to fiber waviness or misalignment. This value will be used in the following analysis.

For the graphene-enhanced composite, again assuming uniform strain, the rule of mixtures gives:

$$E_{comp} = E_{CF}V_{CF} + E_{epoxy}V_{epoxy} + E_fV_f \quad (5)$$

where E_f is the effective Young's modulus of the graphene and V_f is its volume fraction. Assuming that the density of the graphene is similar to that of the epoxy resin matrix and with the value of $E_f \sim 825$ GPa determined from Raman band shifts, a value of $E_{comp} \sim 122.5$ GPa is predicted. This is close to the experimentally-determined value of E_{comp}, 124.1 ± 5.1 GPa. Since the graphene flakes are not perfectly aligned (Fig. 2) the value of $E_f \sim 825$ GPa could be even higher with better alignment. An alternative interpretation could be that the experimentally-determined Young's modulus value of 124.1 GPa for the enhanced composite implies an effective graphene modulus of around 1 TPa, its theoretical value [1]. Similar analysis to the above has also been carried out for the 90° samples, as shown in SI.

The ability of graphene to reinforce a UD composite in the fiber direction is perhaps surprising as the axial Young's modulus is commonly thought to be dominated by the high modulus fibers with the contribution of the low modulus matrix being insignificant (Eq. (5)). It is therefore important to consider the reinforcement of the matrix offered by the presence of the graphene. It was shown in a recent study using shear lag analysis [13] that the filler modulus is given by

$$E_f = E_{gra}\eta_o\left[1\left(-\frac{\tan h(ns/2)}{ns/2}\right)\right] \quad \text{where } n = \sqrt{\frac{2G_m}{E_{gra}}\frac{t}{T}} \text{ and } G_m = \frac{E_m}{2(1+\nu)} \quad (6)$$

The parameters G_m, E_m and ν are the shear modulus, Young's modulus and the Poisson's ratio of the polymer matrix. t is the thickness of graphene and T is the overall thickness of the representative matrix volume element. The aspect ratio of the graphene is s and η_o is the Krenchel orientation factor [9,10].

It has been shown for bulk graphene nanocomposites that Eq. (6) predicts that E_f increases as E_m increases and for low modulus matrix materials $E_f \propto E_m$ as is found experimentally [13]. What is most relevant to this present study is that the graphene is confined in the resin regions between the carbon fibers (Fig. 4) such that the graphene is flattened and aligned ($\eta_o \rightarrow 1$). The variation of E_f with E_m predicted using Eq. (6) is shown in Fig. 7 for different values of t/T using the local matrix modulus of the carbon fiber reinforced composite ($E_m \sim 114$ GPa) rather than that of the resin matrix (~4 GPa). It can be seen that the data point for the value of E_f determined from the Raman bands shifts lies in the range $10^{-2} > t/T > 10^{-3}$. Assuming that the graphene is in the order of 1–2 nm thick, this means that T must be in the range 0.2–2.0 μm, the dimensions of the resin regions between the fibers (Fig. 4 and Fig. S2)

In addition to the increase in axial Young's modulus for the graphene-enhanced composite, there is also an increase in axial strength (Table 1). It appears that this increase in strength is a simple reflection of the increase in stiffness - both increased by the order of 8%. It is also interesting that the addition of the graphene makes little difference to the transverse mechanical properties (Table 1 and SI). This is most likely a result of the high degree of anisotropy in the mechanical properties of the highly-aligned few-layer graphene. Similar improvement has also been reported previously by Leopold et al. [36]. Its transverse stiffness will be similar to that of the carbon fibers and a 2% loading in the resin would be expected to give only a slight increase in the transverse (90°) stiffness and strength, as is found.

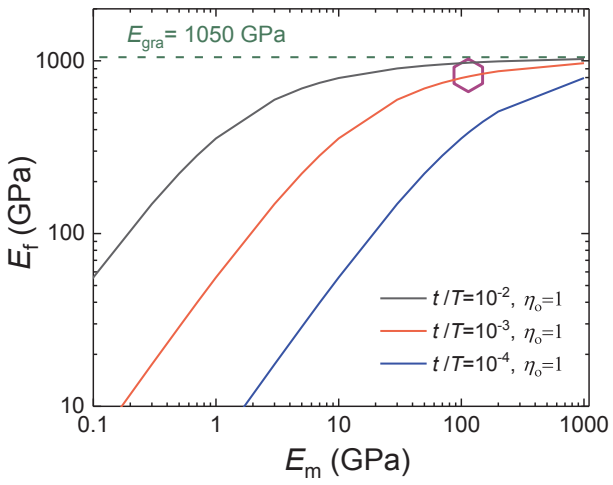

Fig. 7. The variation of E_f with E_m predicted using Eq. (6) for different values of t/T. The data point for the graphene-enhanced composite is shown as the hexagon. (For interpretation of the references to colour in this figure legend, the reader is referred to the web version of this article.)

4. Conclusions

In conclusion, a graphene-enhanced unidirectionally-reinforced carbon fiber composite has been prepared and a ~10 GPa increase in the Young's modulus of the fiber direction is obtained with only 2 wt% of graphene in the resin. The effective Young's modulus of graphene has been estimated by Raman spectroscopy to be around 825 GPa, approaching its theoretical limit. It has been demonstrated the enhancement is due to three effects: (1) the alignment of graphene around the fiber by a 'filtering' effect [26]; (2) confinement of graphene between the fiber gaps and (3) the matrix being stiffened by the carbon fibers. It shows the considerable potential of using graphene to enhance the mechanical properties of conventional carbon fiber composites even in the high-stiffness fiber direction.

Acknowledgement

The authors are grateful for the support of the National Graphene Institute of The University of Manchester. The authors thank Dr Teruo Hashimoto at University of Manchester for his kind help on preparing samples for X-ray CT.

Conflict of interest

The authors declare no competing financial interest.

References

[1] Lee C, Wei X, Kysar JW, Hone J. Measurement of the elastic properties and intrinsic strength of monolayer graphene. Science 2008;321(5887):385–8.
[2] Boland CS, Khan U, Ryan G, Barwich S, Charifou R, Harvey A, et al. Sensitive electromechanical sensors using viscoelastic graphene-polymer nanocomposites. Science 2016;354(6317):1257–60.
[3] Papageorgiou DG, Kinloch IA, Young RJ. Mechanical properties of graphene and graphene-based nanocomposites. Prog Mater Sci 2017;90:75–127.
[4] Hu K, Kulkarni DD, Choi I, Tsukruk VV. Graphene-polymer nanocomposites for structural and functional applications. Prog Polym Sci 2014;39(11):1934–72.
[5] Stankovich S, Dikin DA, Dommett GHB, Kohlhaas KM, Zimney EJ, Stach EA, et al. Graphene-based composite materials. Nature 2006;442(7100):282–6.
[6] Dikin DA, Stankovich S, Zimney EJ, Piner RD, Dommett GHB, Evmenenko G, et al. Preparation and characterization of graphene oxide paper. Nature 2007;448(7152):457–60.
[7] Gong L, Kinloch IA, Young RJ, Riaz I, Jalil R, Novoselov KS. Interfacial stress transfer in a graphene monolayer nanocomposite. Adv Mater 2010;22(24):2694–7.
[8] Gong L, Young RJ, Kinloch IA, Riaz I, Jalil R, Novoselov KS. Optimizing the reinforcement of polymer-based nanocomposites by graphene. ACS Nano 2012;6(3):2086–95.
[9] Li ZL, Young RJ, Kinloch IA, Wilson NR, Marsden AJ, Raju APA. Quantitative determination of the spatial orientation of graphene by polarized Raman spectroscopy. Carbon 2015;88:215–24.
[10] Li ZL, Young RJ, Wilson NR, Kinloch IA, Valles C, Li Z. Effect of the orientation of graphene-based nanoplatelets upon the Young's modulus of nanocomposites. Compos Sci Technol 2016;123:125–33.
[11] Leopold C, Augustin T, Schwebler T, Lehmann J, Liebig WV, Fiedler B. Influence of carbon nanoparticle modification on the mechanical and electrical properties of epoxy in small volumes. J Colloid Interface Sci 2017;506:620–32.
[12] Marom G, Daniel Wagner H. Should polymer nanocomposites be regarded as molecular composites? J Mater Sci 2017;52(14):8357–61.
[13] Young RJ, Liu M, Kinloch IA, Li S, Zhao X, Vallés C, et al. The mechanics of reinforcement of polymers by graphene nanoplatelets. Compos Sci Technol 2018;154:110–6.
[14] Qin W, Vautard F, Drzal LT, Yu J. Modifying the carbon fiber–epoxy matrix interphase with graphite nanoplatelets. Polym Compos 2016;37(5):1549–56.
[15] Zhang X, Fan X, Yan C, Li H, Zhu Y, Li X, et al. Interfacial microstructure and properties of carbon fiber composites modified with graphene oxide. ACS Appl Mater Interfaces 2012;4(3):1543–52.
[16] Ning H, Li J, Hu N, Yan C, Liu Y, Wu L, et al. Interlaminar mechanical properties of carbon fiber reinforced plastic laminates modified with graphene oxide interleaf. Carbon 2015;91:224–33.
[17] Pathak AK, Borah M, Gupta A, Yokozeki T, Dhakate SR. Improved mechanical properties of carbon fiber/graphene oxide-epoxy hybrid composites. Compos Sci Technol 2016;135:28–38.
[18] Chen L, Jin H, Xu Z, Shan M, Tian X, Yang C, et al. A design of gradient interphase reinforced by silanized graphene oxide and its effect on carbon fiber/epoxy interface. Mater Chem Phys 2014;145(1):186–96.
[19] Knoll JB, Riecken BT, Kosmann N, Chandrasekaran S, Schulte K, Fiedler B. The effect of carbon nanoparticles on the fatigue performance of carbon fibre reinforced epoxy. Comp Part A 2014;67:233–40.
[20] Ashori A, Rahmani H, Bahrami R. Preparation and characterization of functionalized graphene oxide/carbon fiber/epoxy nanocomposites. Polym Test 2015;48:82–8.
[21] Li Z, Young RJ, Kinloch IA. Interfacial stress transfer in graphene oxide nanocomposites. ACS Appl Mater Interfaces 2013;5(2):456–63.
[22] Malard LM, Pimenta MA, Dresselhaus G, Dresselhaus MS. Raman spectroscopy in graphene. Phys Rep 2009;473(5–6):51–87.
[23] Ferrari AC, Basko DM. Raman spectroscopy as a versatile tool for studying the properties of graphene. Nat Nanotechnol 2013;8(4):235–46.
[24] Ferrari AC, Robertson J. Interpretation of Raman spectra of disordered and amorphous carbon. Phys Rev B 2000;61(20):14095–107.
[25] Okuda H, Young RJ, Tanaka F, Watanabe J, Okabe T. Tensile failure phenomena in carbon fibres. Carbon 2016;107:474–81.
[26] Zhang H, Liu Y, Huo S, Briscoe J, Tu W, Picot OT, et al. Filtration effects of graphene nanoplatelets in resin infusion processes: problems and possible solutions. Compos Sci Technol 2017;139:138–45.
[27] Krenchel H. Fibre reinforcement. Copenhagen: Akademisk Forlag; 1964.
[28] Vallés C, Beckert F, Burk L, Mülhaupt R, Young RJ, Kinloch IA. Effect of the C/O ratio in graphene oxide materials on the reinforcement of epoxy-based nanocomposites. J Polym Sci B Polym Phys 2016;54(2):281–91.
[29] Papageorgiou DG, Kinloch IA, Young RJ. Hybrid multifunctional graphene/glass-fibre polypropylene composites. Compos Sci Technol 2016;137:44–51.
[30] Li Z, Kinloch IA, Young RJ. The role of interlayer adhesion in graphene oxide upon its reinforcement of nanocomposites. Philos Trans R Soc A 2016;374:(2071).
[31] Mohiuddin TMG, Lombardo A, Nair RR, Bonetti A, Savini G, Jalil R, et al. Uniaxial strain in graphene by Raman spectroscopy: G peak splitting, Grüneisen parameters, and sample orientation. Phys Rev B 2009;79(20). 205433.
[32] Lee JE, Ahn G, Shim J, Lee YS, Ryu S. Optical separation of mechanical strain from charge doping in graphene. Nat Commun 2012;3:1024.
[33] Mueller NS, Heeg S, Alvarez MP, Kusch P, Wasserroth S, Clark N, et al. Evaluating arbitrary strain configurations and doping in graphene with Raman spectroscopy. 2D Materials 2018;5(1). 015016.
[34] Li P, Huang T-C, White KL, Hawkins S, Kotaki M, Nishimura R, et al. Spray-coated epoxy barrier films containing high aspect ratio functionalized graphene nanosheets. RSC Adv 2015;5(124):102633–42.
[35] Young RJ, Lovell PA. Introduction to polymers. 3rd ed. Boca Baton (FL, USA): CRC Press; 2013.
[36] Leopold C, Schetle A, Kosmann J, Fiedler B In ply-tailored nanoparticle matrix modification in cross-ply CFRP laminates. In: 21st International conference on composite materials, Xi'an, China; 2017.